SCIENCE BULLETIN
CHIAO TUNG UNIVERSITY
Vol. 5, No. 1, APRIL 1971

MICROWAVE AVALANCHE DIODES*

S. M. Sze+ and R. M. Ryder

Bell Laboratories

Murray Hill, New Jersey, 07974 U.S.A.

ABSTRACT

Microwave avalanche diodes of various types (Impatt, Trapatt, etc.) can generate power sufficient for microwave receivers and some transmitters. This brief review summarizes mechanisms of operation, power output, efficiency, noise, and some important features of design and fabrication.

I. INTRODUCTION

Since the first experimental observation of microwave oscillation from a silicon diode in 1965 by Johnston, De Loach, and Cohen[1], avalanche diodes have become preferred solid-state sources of microwave power. Continuous-wave (CW) power available is sufficient for receivers and some transmitters throughout the microwave frequency range (about 1 GHz to 100 GHz). The power is considerably more than can be obtained from CW Gunn diodes, but at the expense of higher noise and higher operating voltages.

Avalanche diodes can be designed and operating in various modes. The first and the most important mode of operation is called the Impatt mode. The name Impatt is an acronym to recall the major mechanisms of operation first proposed by Read[2] - IMPact Avalanche and Transit Time. Ordinarily the Impatt mode operates with best efficiency near the "transit-time" frequency, and efficiency of DC to RF power conversion is at present limited to about 15%.

---

* An invited paper to be published in Proc. IEEE Special Issue on Microwave Semiconductor Devices, July 1971.

+ Professor at Large, College of Engineering, National ChinoTung University.

A second mode of operation was discovered by Prager, Chang, and Weisbrod[3] in 1967. They called it the "anomalous" mode because the operating frequency is substantially lower than the transit-time frequency. The obtainable efficiency is considerably higher (50%) and a substantial change in DC operating voltage occurs when the diode switches into the mode. Subsequent theoretical studies established[37] the mechanism responsible for the new mode. Under certain conditions of large space charge it can happen that the periodic avalanching of the diode begins at the high-field side and sweeps rapidly across the diode,[39] leaving it substantially filled by a highly conducting plasma of holes and electrons whose space charge depresses the voltage to very low values. Since the plasma cannot rapidly escape, this mode is called the trapped plasma mode or Trapatt mode (for TRApped Plasma Avalanche Triggered Transit).[38]

Other modes of operation[4] have been recognized by some authors as occurring under special conditions in some diodes. A parametric mode can occur when pumped variable reactance effects are prominent, and a thermal mode may appear when frequency is low enough so that diode temperature varies significantly during each cycle of oscillation. A space-charge feedback mode has been described, but of course space-charge effects are prominent in all modes.

We shall consider in the next section the two fundamental physical processes pertinent to the device operation, namely the drift velocity and avalanche multiplication. In Section III the operational principle of the Impatt mode will be considered. The power and efficiency limitations on the Impatt mode are discussed in Section IV. The noise behavior of Impatt diodes is considered in Section V. Section VI presents the operational principle of the Trapatt mode and briefly discusses other modes of operation. Designs and state-of-the-art performances of avalanche diodes as of late 1970 are summarized in Section VII.

II. DRIFT VELOCITY AND AVALANCHE MULTIPLICATION

There are two fundamental physical processes most pertinent to the operation of avalanche diodes: (1) the drift velocity at which carriers travel under the influence of an electric field and (2) the avalanche multiplication which occurs when the electric field in a semiconductor is sufficiently high ($3 - 6 \times 10^5$ V/cm in Si) that the carriers gain enough energy to excite electron-hole pairs by impact ionization.

When the electric field is low, the average drift velocity is directly proportionally to the field and the proportionality constant is called the mobility. As the field increases, the carriers interact more strongly with the lattice (especially in emitting optical phonons), so that the average velocity falls much below a linear projection from low-field values. The measured room-temperature drift velocities[5] for high-purity Ge, Si, and GaAs[6,7] are shown in Fig. 1. We note that for fields above 10^4 V/cm, the drift velocity approaches a limiting value and becomes independent of the field. This value is called the scattering-limited velocity, v_s,

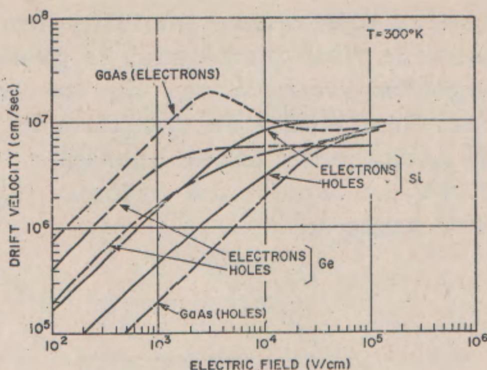

Fig. 1 Drift velocity of charge carriers. At high fields $\sim 10^5$ V/cm, the scattering limited velocity v is nearly independent of field. (Ref. 5, 6, 7)

and is given by [8,9]

$$v_s \cong \sqrt{\frac{8\,E_{op}\,\tanh\,(E_{op}/2kT)}{3\pi m}} \tag{1}$$

where E_{op} is the optical phonon energy, k the Boltzmann constant, T the lattice temperature, and m the mass of the carriers. The values of v_s and E_{op} for the above three semiconductors are listed in Table I along with other parameters. Since all Impatt diodes are operated at temperatures considerably higher than room temperature (300°K), the corresponding v_s will be smaller. For example, at 500°k the scattering-limited velocities as obtained from Eq. (1) are 5×10^6, 9×10^6, and 7×10^6cm/sec for electrons in Ge, Si, and GaAs respectively.

TABLE I. MATERIAL PARAMETERS

Semiconductor	Ge	Si	GaAs
Energy GaP, E_g (300°K) (eV)	0.67	1.12	1.43
Maximum Electric Field at Breakdown, E_m (V/cm)	$2\text{-}3\times10^5$	$3\text{-}6\times10^5$	$3.5\text{-}6.5\times10^5$
Dielectric Constant, ($\varepsilon_s/\varepsilon_o$)	16	11.8	12
Drift Mobility, μ (cm^2/V-sec) Electrons (μ_n) Holes (μ_p)	3900 1900	1500 600	8500 400
Thermal Conductivity, κ (Watt/cm-°K)	0.64	1.45	0.45
Optical Phonon Energy E_{op} (eV)	0.037	0.063	0.035
Scattering-Limited Velocity, V_s (cm/sec) Electrons (300°K) Holes (300°K)	6×10^6 8×10^6	10^7 10^7	9×10^6 9×10^6

The region of negative differential mobility for electrons in GaAs, where velocity decreases as field increases, is prominent in the curves. The corresponding negative conductance, due to "valley transfer", is the operating basis for Gunn and LSA oscillators, but has little or no effect on Impatt diodes because the latter operate mostly at much higher fields of the order of 10^5V/cm where the velocity is essentially constant at the scattering-limited value v_s.

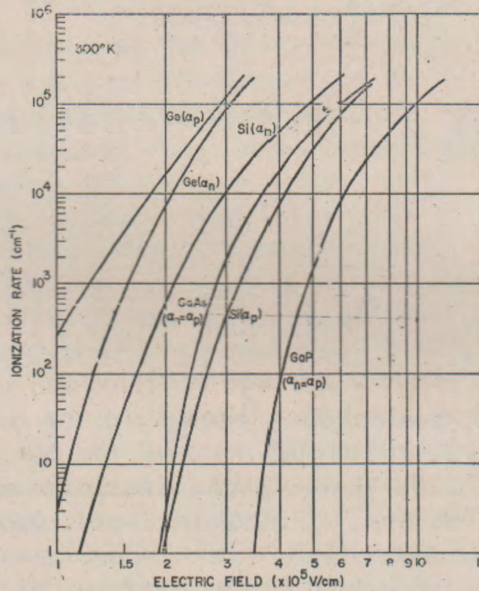

Fig. 2 Ionization rates for avalanche multiplication. For Si, rates for holes and electrons differ drastically; for Ge, GaAs, and GaP, the rates are nearly the same. (Ref. 5)

As the field increases above 10^5 V/cm, impact ionization occurs. The ionization rates are sensitive functions of the field; measured room-temperature results[5] for Ge, Si, GaAs, and GaP are shown in Fig. 2. As we can see, the ionization rate can increase five orders of magnitude for an increase of the field by a factor of only two or three. We also note that the electron ionization rate (α_n) in silicon is substantially larger than that of holes (α_p) while for other semiconductors the electron and hole ionization rates are essentially the same. This fact has special relevance for the noise behavior of Impatt diodes to be considered in Section V.

As the temperature increases, the mean free path for phonon collisions decreases, causing a reduction of the ionization rate. The temperature dependence of the ionization rate can be obtained from the modified Baraff theory.

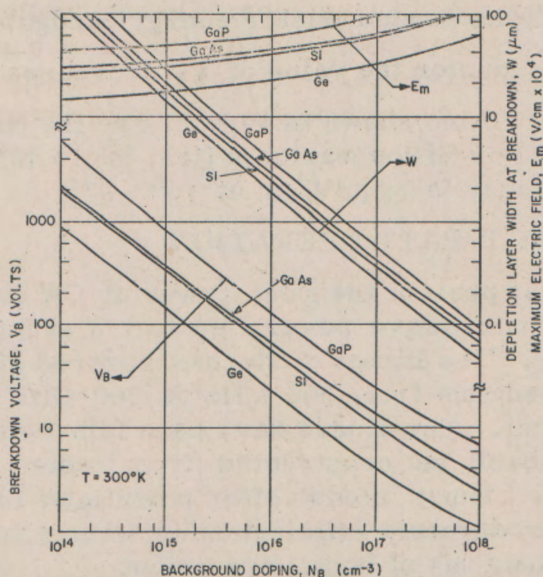

Fig. 3 Breakdown voltage, breakdown field, and depletion-layer width for abrupt p-n junctions. (Ref. 13)

The basic equation which describes avalanche multiplication when it is initiated by electrons is[12]

$$\int_0^W \alpha_n \exp\left[-\int_0^X (\alpha_n - \alpha_p)\, dx'\right] = 1 - \frac{1}{M} \tag{2}$$

where M is the multiplication factor, and W is the depletion width. Self-sustaining avalanche breakdown occurs when M approaches infinity, i.e.

$$\int_0^W \alpha_n \exp\left[-\int_0^X (\alpha_n - \alpha_p)\, dx'\right] dx = 1 . \tag{3}$$

For equal ionization rates, Eq. (3) reduces to

$$\int_0^W \alpha \, dx = 1 . \tag{3a}$$

The above equations are used to evaluate the breakdown voltage, V_B, and the depletion width, W, at breakdown. The results for one-sided abrupt

junctions (and Schottky barrier contacts) are shown[13] in Fig. 3. It is interesting to note that at a given background doping, the breakdown voltage increases with the semiconductor energy bandgap ($V_B \sim E_g^{3/2}$) and for a given semiconductor the value of V_B decreases with increasing doping ($V_B \sim N_B^{-3/4}$). Also shown in Fig. 3. are the maximum electric fields at breakdown. For Si the maximum field is 3×10^5 V/cm at 10^{15} cm^{-3} and increases slowly to 6×10^5 V/cm at 10^{17} cm^{-3}.

III. MECHANISMS OF IMPATT OPERATION

Impatt diodes are at present the most powerful CW solid-state sources of high-frequency microwave power; up to 1 W at 50 GHz has been realized (see Fig. 28). The Impatt diode has covered the complete microwave frequency spectrum from 300 MHz to 300 GHz (or wavelength range from 1 mm to 1 m). The diodes have been fabricated from Ge, Si, and GaAs and can probably be constructed from other semiconductors should the need arise. Impatt diodes offer potentially inexpensive, reliable, compact, and moderately efficient microwave sources. We shall now consider the mechanisms of Impatt operation.

1. Basic Considerations

Many electron-discharge devices may be considered to be analyzable into the following functional parts:

A) A source of carriers.

B) A region where the current of the discharge is modulated by the rf signal.

C) A working region where the carriers produce useful power output by interacting with the rf field.

D) One or more collectors which dispose of the spent carriers.

In Impatt diodes, the source is the region interior to the diode where impact multiplication is appreciable, called the avalanche region. Holes and electrons are produced in practically equal numbers. Since the multiplication is quite sensitive to the magnitude of field present, the avalanche region is also the place where the carrier transport current is modulated by the rf field. The collectors are the diode contacts, at opposite ends of the interaction space. The working region consists of both the avalanche region itself and the "drift" region between the source and collector, where the field may be too low for impact multiplication. The holes and electrons of course drift in opposite directions. Usually there is only one drift region, so that the opposite carriers disappear into their collector without doing much useful work; but recently some "double-drift" diodes have successfully used both holes and electrons (refer to Sec. VII).

Ordinarily the resistance of a slab of semiconductor between electrodes is positive; the electric field is approximately in phase with the current; power is dissipated, not generated. But in a number of different ways, the phase of the current may be shifted to make the resistance

negative. In the Impatt oscillators, the principal phase shift mechanisms are the delays due to finite transit time of carriers and due to finite build-up and decay times of the avalanche-produced carriers.

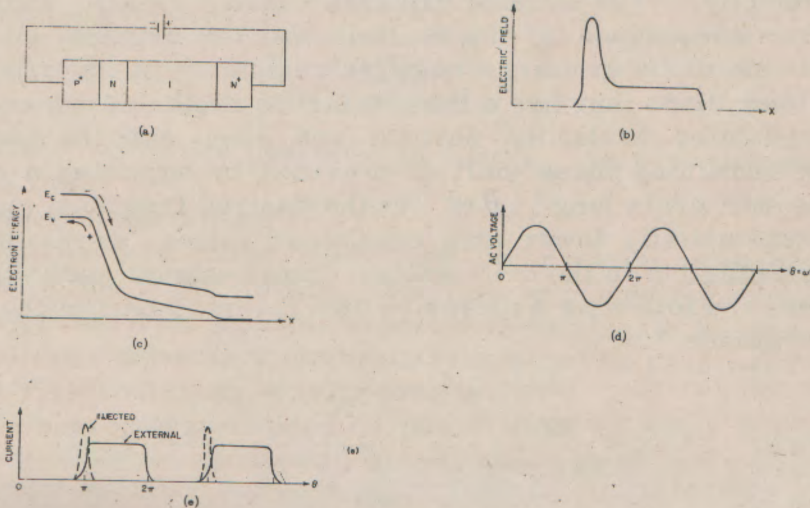

Fig. 4 Read Diode. (a) Structure. (b) Field Profile, showing narrow avalanche region and long drift region. (c) Energy bands. (d) Voltage wave form. (e) Injected current of avalanching carriers compared with induced current in diode electrodes. (After Read, Ref. 2)

Figure 4(a) shows the structure of a Read diode[2] which is basically a p^+nin^+ diode (or its compliment n^+pip^+). The DC electric field profile under reverse-biased avalanche breakdown condition is shown in Fig. 4(b). There is a high-field avalanche region at the p^+n junction where electron-hole pairs are generated and a near constant-field drift space in the intrinsic "i" region. Figure 4(c) shows the energy band diagram under the breakdown condition. The generated holes quickly enter the p^+ region; the generated electrons are injected into the drift space, where they do work which produces external power. As the electric field changes periodically with time around an average value (Fig. 4(d)) the impact ionization rate per carrier follows the field change nearly instantaneously. However, the carrier density does not follow the field change in unison, because carrier generation depends also on the number already present. Even after the field has passed its maximum value, the carrier density keeps increasing because the carrier generation rate is still above the average value. The maximum carrier density is reached approximately when the field has decreased from the peak to the average value. Thus the ac variation of the carrier density lags the ionization

rate by about 90°, although the ionization rate is in phase with the ac field. The above situation is illustrated as the "injected" current in Fig. 4(e). The peak value of ac field (or voltage) occurs at $\theta = \pi/2$, but the peak of the injected carrier density occurs at $\theta = \pi$. The injected electrons then enter the drift region which they traverse at scattering-limited velocity. The induced external current is also shown in Fig. 4(e). From comparison of the ac field and the external current it is clear that the diode exhibits a negative resistance at its terminals.

The Reak diode thus has a thin avalanche region at one end, providing the modulated avalanche current and about half the needed phase shift; the remaining phase shift is provided by adjoining a drift space about one-half cycle long ($\theta = \pi$ at the desired frequency) in which the field is substantially lower than breakdown values, so that impact ionization is negligible in the drift space. Small-signal analysis of a Read diode gives the following expression for the real part of the diode terminal admittance [14]

$$G \sim \frac{W}{A \epsilon_s \omega} \left(\frac{1}{1 - \frac{\omega^2}{\omega_r^2}} \right) \left(\frac{1 - \cos\theta}{\theta} \right) \tag{4}$$

where W is the depletion width, A the diode area, ε_s the dielectric permittivity, θ the transit angle given by $\omega W / v_s$ and ω_r the avalanche resonant frequency given by

$$\omega_r = \sqrt{\frac{2\alpha' \, v_s \, J_o}{\epsilon_s}} \tag{5}$$

in which the quantity α' is the derivative of the ionization rate with respect to electric field and J_o is the dc current density. From Eq. 5, the conductance can only be negative when $\omega > \omega_r$.

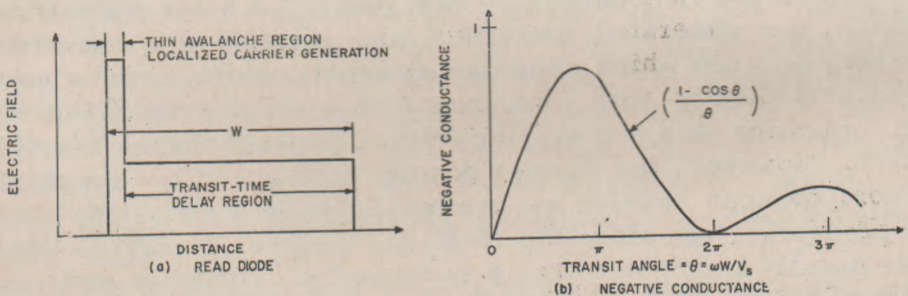

Fig. 5 Read diode. (a) Avalanche and drift regions. (b) Idealized negative conductance vs transit angle.

The variation of the negative conductance with the transit angle is plotted in Fig.5. We note that the peak value occurs near $\theta = \pi$. For transit angles larger than π and approaching $3\pi/2$ the negative conductance of the device decreases rapidly. For practical purposes, although the range of negative conductance may be quite wide, we shall consider that Read-type Impatt diodes work well only in a frequency range around the π transit angle, i.e.,

$$f \cong \frac{v_s}{2W} \tag{6}$$

For example, for 10GHz operation in silicon, the depletion width should be about 5 um.

2. General Considerations[15]

Besides the Read diode there are other varieties of diodes which also belong to the Impatt family. The first reported microwave oscillation was obtained from a simple abrupt p-n junction.[1] Misawa has shown that a negative conductance of Impatt nature can be possessed by a junction diode with almost any doping profile.[16]

To investigate optimization of phase shift between avalanche and transit time, Misawa introduced the concept of "uniform" avalanching and analyzed it by small-signal methods. Misawa showed that a uniformly avalanching region-one in which the rate of carrier production by impact ionization is constant throughout - can exhibit a small negative conductance all by itself, without any additional "drift" region. The equivalent circuit shows that for small signals the avalanche can be represented as an electronic admittance roughly proportional to bias current. The electronic admittance, in shunt with the usual depletion layer capacitance, consists of a negative conductance shunted by an inductive susceptance which is an order of magnitude larger, in agreement with Read's suggestion that the phase lag of the current is approximately 90°. The avalanche resonant frequency can thus be defined by the shunt combination of the depletion layer capacitance and the avalanche inductive susceptance; it increases approximately as the square root of bias current (Eq. 5). The negative conductance, as a function of frequency, is nearly constant for frequencies up to transit angle $\theta = 2\pi$; thereafter it shows transit-time -like variations. Both conductance and susceptance are roughly proportional to bias current. This combination of properties, applying to a uniformly avalanching diode, may be collectively labeled by the term "Misawa diode."

The electric field profiles for the Read diode, p-n junction and Misawa diode are shown in Fig. 6(a). The abrupt p-n junction can be classified as a Read-type diode, since the effective avalanche region of a p-n junction is also very narrow due to the strong dependence of α on the field. The Misawa diode is approximated by a p-i-n diode in which the field is essentially constant.

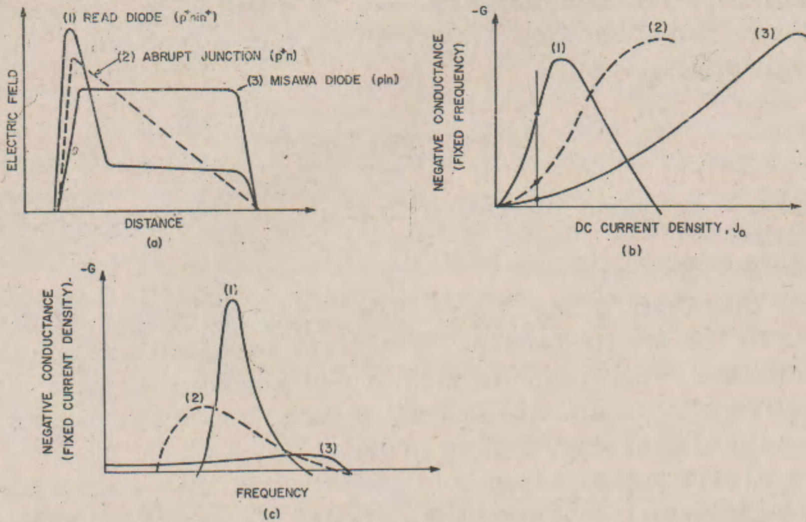

Fig. 6 Effect of doping profile on electric field and conductance for (1) Read, (2) abrupt; (3) Misawa (uniform avalanche) profiles. (a) Electric field at low currents shows narrow avalanche, wide drift for (1) and (2); opposite for (3). (b) Negative conductance vs dc current at a fixed frequency. (c) Read negative conductance is sharply peaked at the "transit-time frequency" where Misawa negative conductance is broad and flat, and extends to zero frequency.

The negative conductance at a fixed operating frequency for the above three structures is shown schematically in Fig. 6(b) as a function of the biasing dc current density. We note that the negative conductance for a Read diode rises to a maximum value at a relatively low current density, then decreases, and eventually disappears at a current density at which the avalanche resonant frequency (which is proportional to $\sqrt{J_o}$, Eq. 5) equals the operating frequency. Similar behaviors are obtained for the other structures. However, the conductance at low current density is smaller and the peak negative conductance occurs at larger current density, for the abrupt junction. Even larger current density is needed for the Misawa diode.

For a fixed current density, the negative conductance vs. operating frequency for the above structures is shown in Fig. 6(c). The Read diode has a relatively narrow peak around the transit-time frequency (Eq. 6). A wider frequency range is obtainable from the abrupt p-n junction with some reduction of peak conductance value due to nonoptimum

phase relation. The reason that the negative conductance disappears at low frequencies (small θ) is that space charge in the drift space can exhibit a large positive resistance at low frequencies.[17] The Misawa diode, however, exhibits a small negative conductance, nearly constant from zero frequency up to the $\theta = 2\pi$ frequency.

These features are observable in practical Impatt diodes provided that space charge is not too large. At large current densities, however, the uniform avalanche model becomes inaccurate. For accurate comparison of practical diodes with theory it is necessary to use numerical

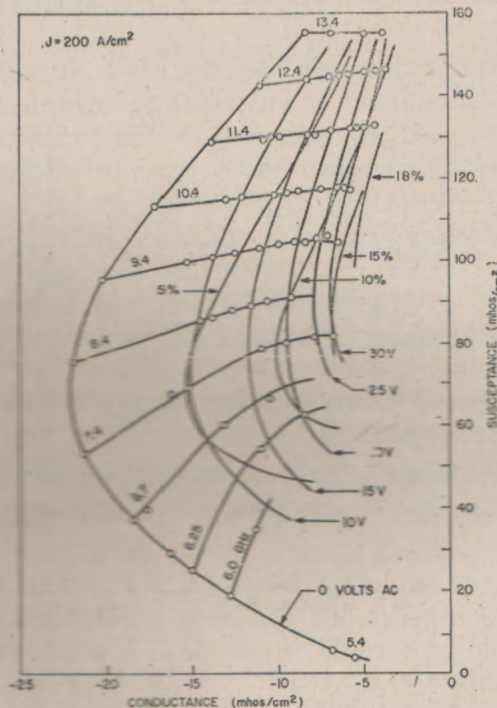

Fig. 7 Numerical calculations of negative conductance and susceptance Note susceptance is very large and strongly current dependent; (After Scharfetter and Gummel, Ref. 18)

computations. An example is shown in Fig. 7 in which both the susceptance and the negative conductance are presented for various ac voltages.[18] Also indicated on the plot are the calculated efficiencies. Note

that generally the susceptance increases with increasing ac voltage amplitude whereas the negative conductance decreases. The calculated result shows efficiencies as high as 18%. Such high efficiency, however, has not been obtained experimentally from diodes operated in the Impatt mode. The limitations on efficiency and power output will now be considered.

IV. POWER AND EFFICIENCY LIMITATIONS

1. Power-Frequency Limitation - Electronic

Because of the inherent limitations of semi-conductor materials and the attainable impedance levels in microwave circuitry, the maximum output power at a given frequency of a single diode is limited. The limitations on semiconductor materials are (1) the critical electric field, E_m, at which the avalanche breakdown occurs and (2) the scattering-limited velocity, v_s, which is the maximum attainably velocity in the semiconductor.

The maximum voltage that can be applied across a semiconductor sample is limited by the breakdown voltage which, for a uniform avalanche, is given by $V_m = E_m W$ where W is the depletion width. The maximum current that can be carried by the semiconductor sample is also limited by the avalanche breakdown process, because of the fact that the current in the space charge region causes an increase of the electric field (from Poisson's equation). With the maximum field again given by E_m, we obtain $I_m = E_m \varepsilon_s v_s A/W$. Therefore, the upper limit on the power input is given by the product of V_m and I_m.

$$P_m = V_m I_m = E_m^2 \quad \epsilon_s v_s A \tag{7}$$

The capacitance associated with a depletion region of W is $C = \varepsilon_s A/W$. Using the transit-time frequency defined in Eq. (6), Eq. (7) can be rewritten as[19]

$$P_m f^2 = E_m^2 \; v_s^2 / \, 8 \pi X_c \tag{8}$$

where X_c is the reactance $(2\pi fc)^{-1}$. Assuming we are limited to some minimum circuit impedance, Eq. (8) predicts that the maximum power which can be given to the mobile carriers decreases as $1/f^2$. This electronic limit is dominant at high frequencies. ($\gtrsim$100GHz in Si).

2. Thermal Limitation on Power Output

At lower frequencies, the CW performance of an Impatt diode is mainly limited by thermal considerations, i.e., by the power which can be dissipated in a semiconductor chip. A typical device mounting arrangement[20] is shown in Fig. 8(a). The cylindrical semiconductor wafer is metallized and attached to a larger metal stud which serves as a heat sink. The heat is generated in the high field region in the semiconductor. The thermal resistance, R_T (in units of C/Watt), consists of three com-

ponents: (1) the effective thermal resistance of the semiconductor approximately, $\frac{W}{2A\sigma_s}$, where A is the diode area and σ_s the semiconductor thermal conductivity, (2) the contacting area component which is proportional to $1/A$, and (3) the spreading resistance component of the heat sink $1/2D\sigma_c$ where D is the diameter.

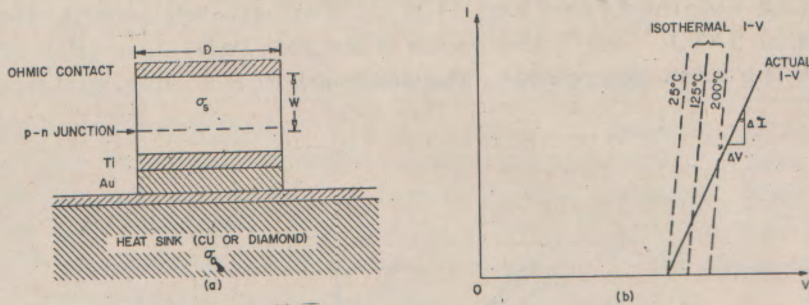

Fig. 8 Thermal considerations. (a) Structure. (b) Strong influence of temperature rise on reverse current voltage characteristic. (After Swan et al., and Gibbons and Misawa, Ref. 20, 21)

The power, P, which can be dissipated in the diode must be equal to the heat power which can be transmitted to the heat sink, therefore, $P=\Delta T/R_T$ where ΔT is the temperature difference between the junction and the heat sink, and R_T is the total thermal resistance. If the reactance $2\pi fC$ (where $C=A\varepsilon_s/W$) is maintained constant, and the major contribution to the thermal resistance is from the semiconductor, then we obtain for a given temperature increase, ΔT:

$$Pf = \left(\frac{\Delta T}{R_T}\right) f \sim \frac{\sigma_s \Delta T}{\epsilon_s} = \text{constant}. \tag{9}$$

So that under the above conditions, the CW power output will decrease as $1/f$.

The thermal resistance can be obtained from DC measurement. Fig. 8(b) shows a typical current-voltage characteristic.[21] Also shown are the isothermal curves at three temperatures. The slope of the isothermal curve is given by the space-charge resistance, R_{sc}, which is $(W-W_A)^2/2A\sigma_s v_s$ where $(W-W_A)$ is the drift space width. As the applied voltage increases, the current, due to avalanche multiplication, will increase; this in turn causes the junction temperature to rise. Sinco the avalanche breakdown voltage increases with increasing temperature, the V-I expression can be written as [22]

$$V = R_{sc} I + V_B (1 + \gamma \triangle T) \tag{10}$$

where V_B is the breakdown voltage at a reference temperature (e.g., 300°K) and γ is the temperature coefficient of breakdown voltage. For small temperature rise $V \approx V_B$, we obtain from the slope:

$$\frac{dV}{dI} = R_{sc} + \gamma R_T \; V_B^2 \tag{10a}$$

The value of γ can be obtained from theoretical or experimental study; and R_T can be obtained from Eq. (10a). For silicon Impatt diodes with device area of 5×10^{-4} cm^2, the value of R_T generally lies between 5-20°C /Watts. As the area decreases, the thermal resistance will accordingly increase.[20]

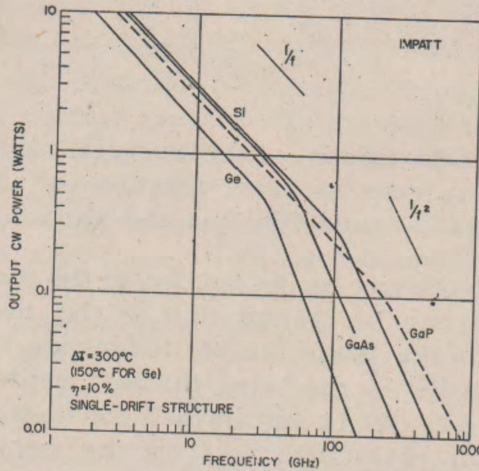

Fig. 9 Calculated power dissipation capability versus frequency. 1/f slop indicates thermal limitation; 1/f slope indicates electronic limitation. For GaP, v_s is assumed to be 10^7 cm/sec. If the maximum temperature difference T is limited to 200°C, the curves in the thermal limitation region should be lowered by about 30%. From Eq. (9). (After Scharfetter, Ref. 23)

The computed results[23] for CW output versus frequency based on the previous considerations are shown in Fig. 9. The maximum temperature rise $\triangle T$ is assumed to be 300°C for Si, GaAs, and GaP, and 150°C for Ge. We note that at lower frequencies we have thermal limitation ($P \alpha 1/f$) and at higher frequencies we have electronic limitation ($P \alpha 1/f^2$). The corner frequency for a given semiconductor depends on the maximum allowed temperature rise and minimum attainable circuit impedance.

3. Limitations on Efficiency

Efficiency is the ratio of ac power output to the power delivered by the dc voltage or current source; therefore

$$\eta = \frac{P_{ac}}{P_{dc}} = (\frac{V_a}{V_d})(\frac{I_a}{I_d}) \tag{11}$$

Under the sharp-pulse approximation[2] of the idealized Read Impatt diode (Fig. 4(e)), we have $(V_a/V_d) \cong \frac{1}{2}$ and $I_a/I_d \cong 2/\pi$; so that the efficiency would be $1/\pi$ or over 30%.

However, for practical Impatt diodes there are many factors which cause significant reduction of the efficiency. These factors include the space-charge effect, the reverse saturation current,[24] the series resistance of the unswept epitaxial layer,[25] the minority injection current,[26] the high-frequency effect (skin effect),[27] and the high field effect (tunneling[28] and saturation of ionization rates).[29] We shall briefly consider the above effects on efficiency.

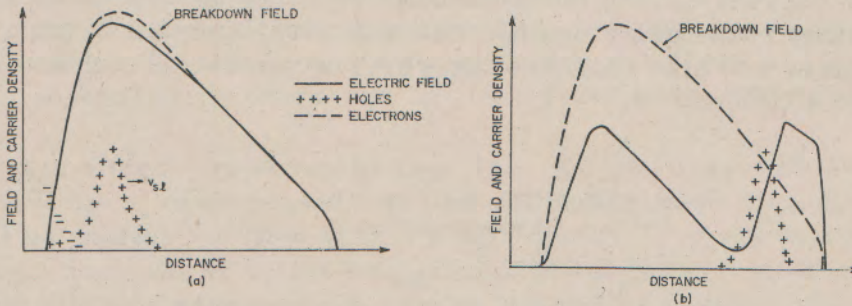

Fig. 10 Instantaneous field and charge distributions in a Read-type Diode. (a) Avalanching just completed, charge beginning to move across diode. (b) Charge transit nearly complete. Note strong effect of space charge in depressing electric field. (After Evens, Ref. 42)

The space-charge effect[15(d)] is shown in Fig. 10. The generated holes will cause a depression of the field by the space charge, Fig. 10(a) The reduction in field may turn off the avalanche process prematurely and thus reduces the 90° phase delay provided by the avalanche. As the holes drift to the right (Fig. 10b), the space-charge may also cause the field to the left of the carrier pulse to drop below that required for velocity saturation. This, in turn, will change the terminal current waveforms and reduce the power generated at the transit-time frequency.

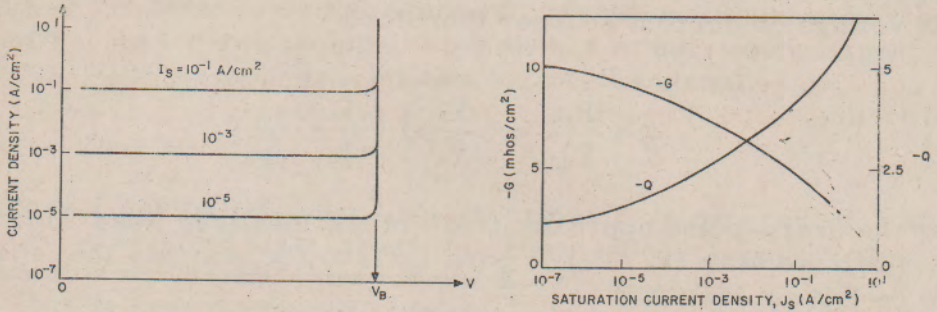

Fig. 11 High saturation current tends to depress oscillation capability. (a) Direct current vs voltage; (b) Negative conductance and Q vs saturation current density. (After Misawa, Ref. 24)

The reverse saturation current effect[24] is shown in Fig. 11. As the current increases, the negative conductance decreases and the negative Q (ratio of susceptance to conductance) increases, causing a reduction of the efficiency. Physically, the difficulty results because a higher saturation current causes the avalanche to build up too soon, reducing the avalanche phase delay again. The minority injection[25] from a poor ohmic contact will also increase the reverse saturation current and thus reduce the efficiency.

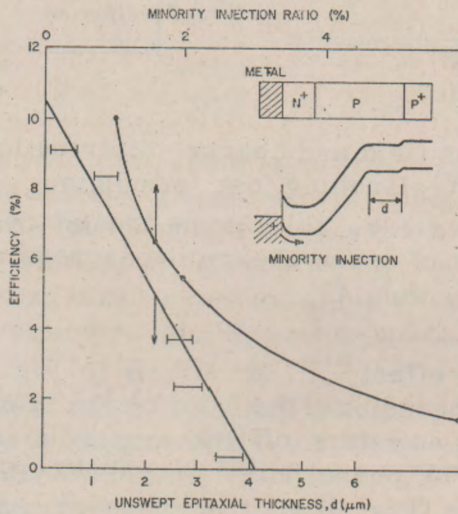

Fig. 12 Effects of unswept epitaxial layer and minority carrier injection. (After Korel and Gibbons, and Dekker et al., Ref. 25, 26)

The effects of an unswept epitaxial layer[26] and the minority injection current[26] are shown in Fig. 12. The unswept layer of thickness d (shown in the insert) gives rise to a series resistance which reduces the terminal negative resistance. In the example shown the efficiency drops from 10% to 2% with 3 um of unswept layer.

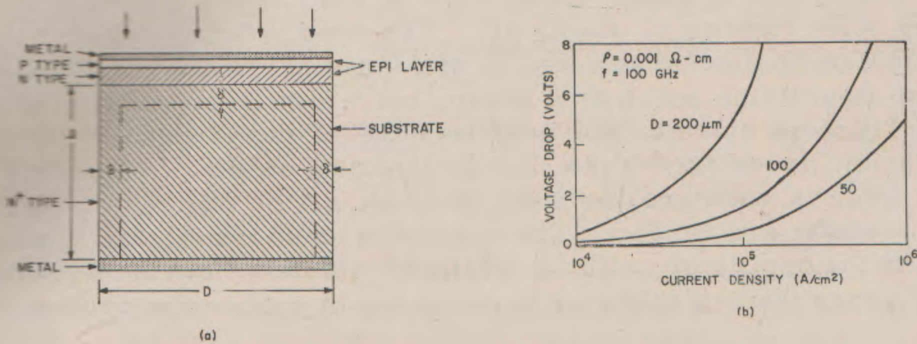

Fig. 13 Skin effect. (a) Current flow is confined to a surface lamina of thickness δ causing nonuniformity and resistive loss in the diode. (b) Calculated voltage drop in substrate at 100 GHz for several diode diameters D. (After DeLoach, Ref. 27)

The skin effect[27] is shown in Fig. 13. As the operating frequency of an Impatt diode is increased into the millimeter wave region, the current will be confined to flow within a skin depth, , of the surface of the substrate. Thus the effective resistance of the substrate is increased and there will be a voltage drop across the radius of the diode as shown in Fig. 13(b). This will cause nonuniform current distribution in the diode and an effective series resistance, both of which reduce efficiency.

For very high frequency operation, the depletion width becomes very narrow,[28] and the field required for impact ionization may exceed 10^6 V/cm. There are two major effects at such high fields. The first one is that tunneling current which may be dominant; since it is in phase with the field, the 90° avalanche phase delay is not provided. The second effect is the saturation of the ionization rates, i.e., the rates will vary slowly as the field increases beyond 10^6 V/cm (refer to Fig. 2). This will cause a broadening of the injected current pulse, and change the terminal current waveform so that the efficiency is reduced.

4. Burnout from Filament Formation[29]

Burnout may occur not only if the diode is overheated but also, more insidiously, if the carrier current fails to be uniformly distributed over the diode area but instead concentrates into filaments of locally high intensity. Such untoward behavior can often result when the diode has a DC negative conductance, because then the local region of greatest cur-

rent density has also the lowest breakdown voltage. For this reason, p-i-n diodes are prone to easy burnout. The moving carrier space charge of drift regions tends to prevent low-frequency negative conductance (Eq. 10) and therefore helps to prevent filamentary burnout. Some diodes which have positive DC conductance at low currents may develop negative DC conductance and burnout at high currents.

V. NOISE BEHAVIOR

The noise level of Impatt oscillators is very high, corresponding to amplifier noise figures of 20-40 dB. The reason for such high noise is that an avalanche discharge consists of a large number of carriers which cross the interaction space as a group, but whose time position "jitters" in phase from one cycle to the next because of the random way in which the avalanche grows from a few initial ionizing events. Therefore this "jitter" noise is much greater than shot noise, in which the individual carrier transits are random. The avalanche noise can be greatly reduced by driving the oscillator with a smaller, quieter "looking" oscillator which triggers the avalanche more uniformly in successive cycles.

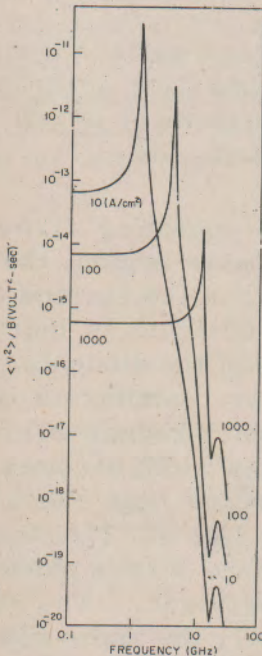

Fig. 14 Calculated equivalent noise voltage vs frequency. The peak at the avalanche fre quency and the dip at twice the transit time frequency are really reflections of corresponding changes in diode impedance. The output noise power varies more smoothly with frequency. (After Gummel and Blue, Ref. 31)

The noise has been quantitatively analyzed in small-signal theories, analytically by Hines[80] and numerically by Gummel and Blue.[31] For a high-gain amplifier under simplified assumptions, the noise figure is[80]

$$NF = 1 + \frac{qV_A/KT_o}{4\,m\,\tau_A^2\,(\omega^2 - \omega_r^2)} \tag{12}$$

where V_A is voltage and τ_A the transit-time across the avalanche region, and m is an exponent which describes approximately the field dependence of impact ionization, i.e., $\alpha=\alpha_0(E/E_0)^m$. The plot of mean-square noise voltage per unit bandwidth versus frequency for a particular silicon diode [31] is shown in Fig. 14. The two theories agree qualitatively in showing a peak of noise voltage at the avalanche resonant frequency ω_r, falling off rapidly at higher frequencies. Noise can therefore be reduced somewhat by operating well above the avalanche frequency and keeping the current low. These conditions are in conflict with the conditions favoring high power and efficiency so that tradeoffs are necessary to optimize for particular applications.

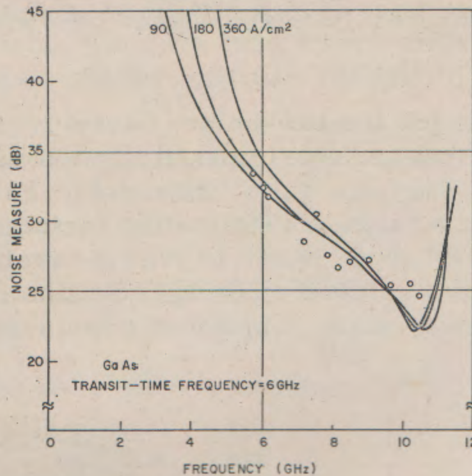

Fig. 15 Noise measure for GaAs Impatt diodes. (After Blue, Ref. 32)

Figure 15 shows theoretical and experimental results of the noise measure in a GaAs Impatt diode.[32,32a] At the transit-time frequency (6 GHz) the noise measure is about 32 dB. The minimum noise measure of 22 dB, however, is obtained at about twice the transit-time frequency. One important feasture of the GaAs noise measure is that it is substantially lower than that for Si Impatt diodes. Table II shows some of the state-of-the-art noise measures of Ge, Si, and GaAs Impatt diodes. The amplifier and oscillator noises in the table are for a lossless circuit at the frequency corresponding to maximum oscillator efficiency, without harmonic turning.

TABLE II. NOISE MEASURE OF IMPATT DIODES

Semiconductor	Ge	Si	GaAs
Small-Signal* Noise Measure (dB)	30	40	20
Large-Signal Oscillator Noise Measure (dB)	40	55	35

*For Small-Signal Amplifier, the Noise Measure is $M=T/T_o$ where $T_o=290^\circ K$.

Oscillator FM Noise is given by

$$\triangle f_{rms} = \left(\frac{f_o}{Q_{ext}}\right)\left(\frac{KT_oMB}{P_o}\right)^{1/2}$$

where f_o=oscillator frequency, Q_{ext}=external circuit Q, M=the large signal noise measure, B=measurement bandwidth, and P_o=oscillator power output.

The main reason for the low-noise behavior in GaAs is that for a given field the electron and hole ionization rates are essentially the same in GaAs while is Si they are quite different. From Eq. (2) it can be shown that to obtain a large multiplication factor M the average distance of ionization $1/\langle\alpha\rangle$ is about equal to W_A (the avalanche width) if $\alpha_n=\alpha_p$, but is about equal to $W_A/\ln M$ if $\alpha_n \gg \alpha_p$. So that for a given W_A there have to be considerably more ionization events in Si, which results in higher noise.

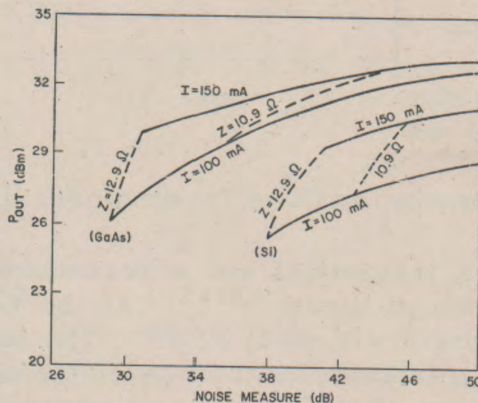

Fig. 16 Noise versus output power for a phase-locked oscillator. Locking power was held constant at + 4 dbm. Contours of constant load impedance Z and constant diode current I are shown. (After Irvin et al., Ref. 34)

The relation between power output and FM noise measure is shown in Fig. 16 for some Si and GaAs 6 GHz Impatt diodes.[34] The diodes were evaluated in a single tuned coaxial resonator circuit in which the load resistance presented to the resonator was incrementally varied by using interchangeable impedance transformers Z. At maximum power output the noise measure is relatively poor. Lower noise measure can be realized at the expense of a slightly reduced power output. We note again that at a given power level (say 1 W) the GaAs Impatt diode is about 10 dB quieter than a Si Impatt diode.

VI. MECHANISMS OF TRAPATT OPERATION AND OTHER MODES OF OPERATION

1. Trapatt Mode

The trapped plasma or Trapatt mode is a high-power high-efficiency mode. To date the highest pulse power of 1.2 kW has been obtained at 1.1 GHz (5 diodes in series)[35] and the highest efficiency[36] of 75% has been obtained at 0.6 GHz. However, the Trapatt operation is a rather complicated manner of oscillation and requires good control of both device and circuit properties. In addition, the Trapatt mode generally shows considerably higher noise measure than Impatt mode; and the upper operating frequency seems to be practically limited to below the millimeter wave region.

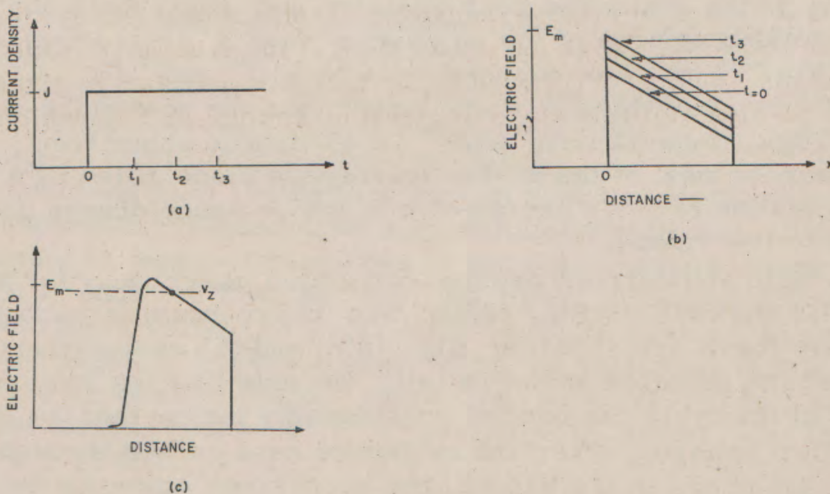

Fig. 17 Trapatt mode operation (schematic). (a) Current density versus time. (b) Idealized electric field rising with time. (c) Avalanche shock front which sweeps through the diode with velocity v_z greater than the scattering-limited velocity v_s. (After Clarfeine et al., DeLoach and Scharfetter, Ref. 40, 41)

To understand the initiating of the Trapatt mode, we consider a current step which is applied at t=o to a n^+pp^+ diode, Fig. 17(a). If at t=o the maximum electric field of the diode is smaller than the critical field E_c at breakdown, the field profile will at first move up with time as shown in Fig. 17(b). This is because[37-41]

$$J = \epsilon_s \frac{dE}{dt} \tag{13}$$

Hence the field can be expressed as

$$E(x,t) = E_m - \frac{qN_A}{\epsilon_s} x + \frac{Jt}{\epsilon_s} \tag{14}$$

where N_A is the doping concentration of the p region. Thus the value of t at which the electric field reaches E_m at a given distance x into the depletion region is obtained by setting $E(x,t)=E_m$, yielding

$$\frac{qN_A x}{\epsilon_s} = Jt \tag{15}$$

or, upon differentiation

$$v_z = \frac{dx}{dt} = \frac{J}{qN_A} \tag{16}$$

where v_z is the avalanche zone velocity and represents the velocity at which the leading edge of the avalanche region progressed through the diode, Fig. 17(c). For example, for $N_A = 10^{15}$ cm^{-3} and $J=10^{14}$ A/cm^2, $v_z = 6\times10^7$ cm/sec which is much larger than the scattering-limited velocity. Thus, the avalanche zone[39] (or avalanche shock front) will quickly sweep across most of the diode, leaving the diode filled by a highly conducting plasma of holes and electrons whose space charge depresses the voltage to low values.[37,38]

The field and carrier density calculated numerically for a particular moment is shown[42] in Fig. 18(a). The corresponding voltage and current wave forms are shown in Fig. 18(b) and (c) respectively. (The dot indicated the situation shown on (a)). We note that the voltage at the beginning of the cycle can become considerably larger than the steady-state breakdown voltage. After the avalanche zone passes through the device the voltage drops to low values, but soon rises again as the field polarizes the space charge. Because of the dependence of the drift velocity on field at low fields (Fig. 1), the electrons and holes will drift at velocities determined by the low-field mobilities, and the time of transit of the carriers can become much longer than W/v_s.

Thus the Trapatt Mode can operate at comparatively low frequencies since the discharge time of the plasma, i.e., the ratio Q/I of its charge

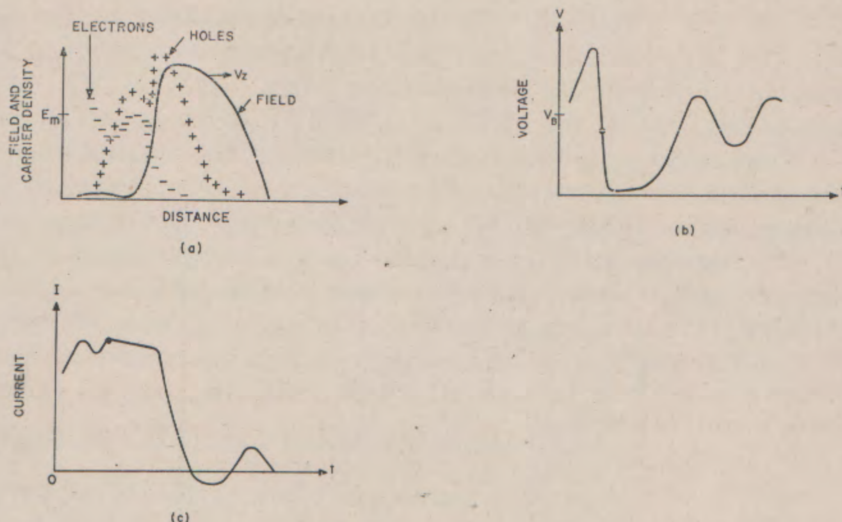

Fig. 18 Trapatt mode operation. (a) Numerical calculation of instantaneous field and charge. (b) Voltage versus time. (c) Current versus time. Dots on voltage and current curves apply to condition shown in (a). (After Evans, Ref. 42)

to its current, can be substantially greater than the nominal transit time W/v of the diode at high fields. Therefore the Trapatt mode is still a transit-time mode in the real sense that the time delay of carriers in transit, i.e. the time between injection and collection, is utilized to obtain current phase shift favorable for oscillation.

The Trapatt mode also requires a circuit which can support harmonics of the fundamental frequency at high voltage amplitudes. The rich harmonic content is necessary in order to get the requisite phase delay in the current at such low frequencies; the diode must not breakdown when the fundamental voltage is a maximum, but is required instead to wait until approximately 1/4 cycle later, when the avalanche is triggered by a peak in the harmonic voltage. Since the terminal voltage can be small when the terminal current is large and vice versa, the Trapatt mode can have high efficiency.

The numerical Fourier analysis of the resulting voltage waveforms based on a step terminal current can give the oscillator power, efficiency, and impedance. Figure 19 shows the theoretical power vs. frequency behavior that one might expect from this mode of operation.[43] Efficiencies substantially higher than 50% have been predicated for some silicon diodes. (75% has been obtained in some UHF avalanche diodes.[36])

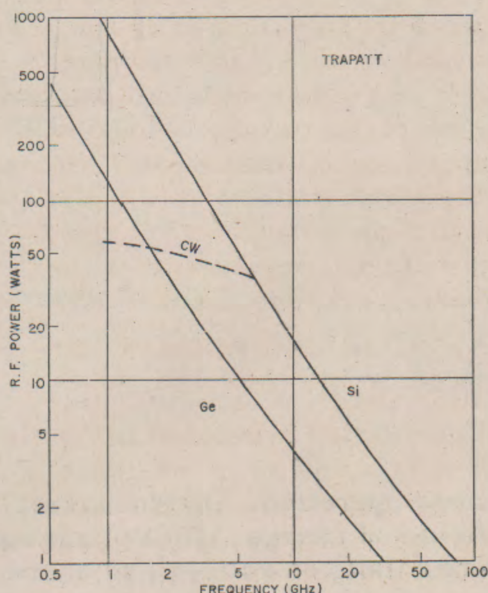

Fig. 19 Theoretical Trapatt power versus frequency. (After Scharfetter, Ref. 43)

2. Other Modes of Operation [4]

As noted in Section III, an avalanche diode can exhibit large electronic susceptances which are strongly current dependent and have low or even negative loss. Consequently they can exhibit parametric amplification, in which gain or oscillation can be obtained by "pumping" the low-loss variable reactance at a high frequency. Such "parametric" amplification is really that of a regenerative reactive modulator, operating between a signal frequency S and a lower sideband (usually (S-b) of the pump frequency b). It is also a complicated form of amplification possibly involving harmonics, since finite impedances and finite voltages must be present at the signal frequency S, the "idler" frequency S-b, the pump frequency b, and possibly also other frequencies. oscillations of variable-reactance type were first observed in Impatt diodes by De Loach, et al,. [4,44] Reactance amplifiers have been built and measured by Hoefflinger, et al, [45] who has noted that at high power levels the various frequencies lock into synchronism and become harmonically related. Under these conditions the parametric amplifier was "self-pumped" - that is, it generated its own pumping frequency.

Another mode of operation is the static mode[46] which may occur in a p-i-n diode. The reverse current-voltage characteristic exhibits a diffe-

rential dc negative resistance. This mode of operation is belived to be of limited usage, since the lack of space charge resistance (Eq. 10) has an important consequence of undesirable nature: there is severe danger of easy burnout by current filament formation at high current densities. (See Sec. IV. 4) This is the reason that all practical avalanche diodes are always designed to include some drift space with finite doping so that some space-charge protection against burnout is obtained.

The thermal mode is another mode of operation, in which the phase shift accompanying temperature rise is important to the operation. However, it is handicapped by two fundamental limitations: (1) it may form filaments as does the static mode, and (2) it is limited in operating frequency by the thermal time constant. Nevertheless it is important to avalanche diode design in that it represents a self-destruction mechanism which must be avoided.

VII. DEVICE DESIGN AND PERFORMANCE

1. Device Fabrication and DC Characteristics

Based upon the discussion presented in Section IV, Impatt diodes are usually designed in such a way as to maximize power output and efficiency. Figure 20 shows some typical high-power Impatt diode designs.

The configuration of Fig. 20(a) is formed by using a double epitaxial process or by diffusion into an epitaxial layer.[47] The n^+ substrate is used to reduce series resistance; and the epitaxial layer thickness should also be controlled so that at breakdown there is essentially no unswept epitaxial layer left. In other words, the depletion layer width at breakdown should be very close to that shown in Fig. 3. For high frequency operation even the n^+ substrate should be thinned down[48] to the order of a few micrometers in order to reduce losses and non-uniformity from skin effect.

Figure 20(b) shows a Schottky barrier Impatt diode.[49,50] A Schottky barrier is a rectifying metal-semiconductor contact.[5] Although the field distributions of Fig. 20(a) and (b) are very similar, the Schottky barrier can offer some unique advantages. One is that the maximum field occurs at the metal-semiconductor interface and the generated heat can be readily conducted away from the metal contact. As shown in Fig. 20(b) the device can be formed in a truncated cone shape[34] so that the high-field singularity at the periphery is removed and uniform breakdown can be obtained inside the device. Another advantage of the Schottky barrier approach is that the device can be fabricated at relatively low temperatures such that the original high quality epitaxial layer can be preserved.

The Schottky barrier approach can also be used in modified Read diode structures[51] as shown in Fig. 20(c) by replacing the p^+ layer by the metal contact. Since the Schottky barrier is basically a majority-carrier device, the minority carrier storage effect,[52] which occurs in the original Read structure, is eliminated and improved efficiency can be achieved.

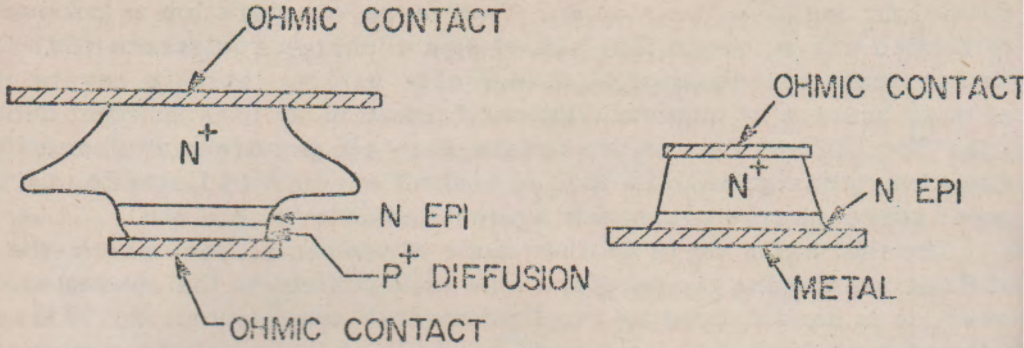

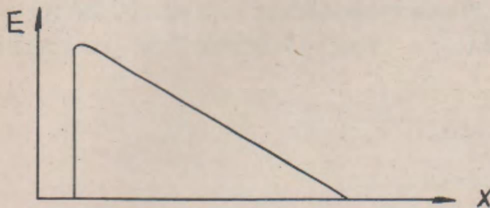

(a) DIFFUSION OR DOUBLE EPITAXIAL

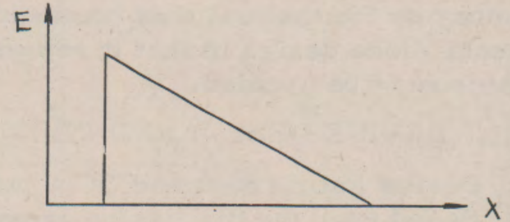

(b) SCHOTTKY BARRIER

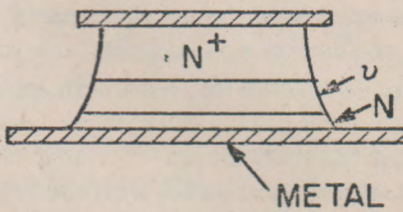

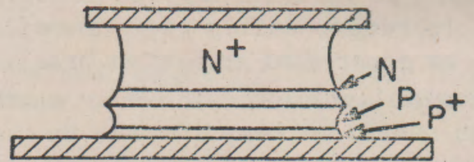

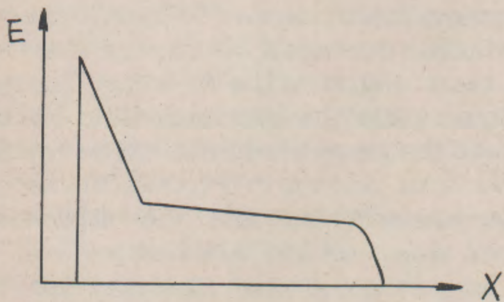

(c) IMPROVED READ DIODE

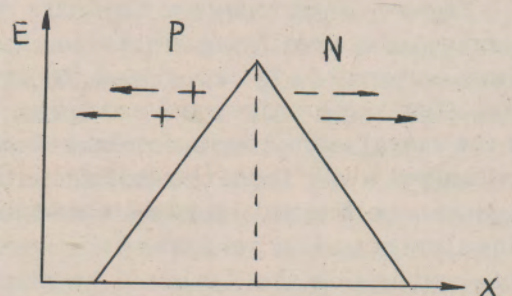

(d) ION IMPLANTATION

Fig. 20 Outlines of some diode shapes and corresponding field profiles. (a) Diffusion or double epitaxial. (After Misawa, Ref. 47) (b) Schottky barrier. (After Irvin et al., Ref. 34) (c) Improved Read diode. (After Misawa, Ref. 51) (d) Ion implantation. (After Scharfetter et al., Ref. 53)

Figure 20(d) shows a new device configuration by using ion implantation technique.[53] For the most common dopants, e.g. B and P, the depth of ion penetration is of the order of 0.5 m/100 KeV, so that 1 μm depth can be readily obtained from ion implantation equipment with a few hundred KeV energy sources. These energy ranges are thus useful in making millimeter wave Impatt diodes. Of particular importance is the possibility of making "double drift" structures as shown in Fig. 20(d) which is much like two complementary Impatt diodes in series, using both types of carriers from the same avalanche source. Power output per unit area and impedance per unit area are both approximately doubled. This structure is thus expected to have increased power output with improved efficiency.[54]

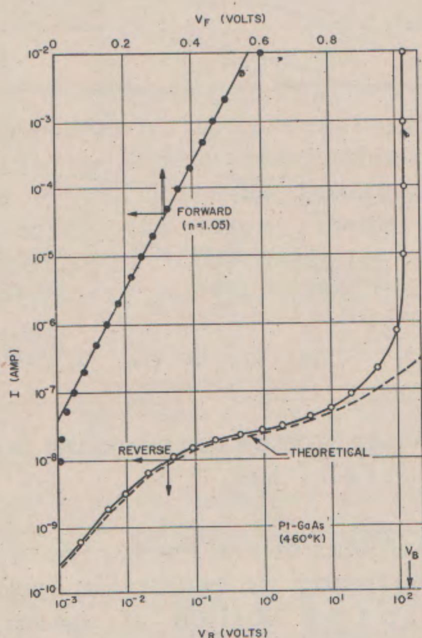

Fig. 21 Current-voltage characteristic of a GaAs Schottky barrier is close to the ideal thermionic-emission theory. (After Coleman et al., Ref. 55)

The DC characteristics of some Schottky barrier diodes correspond closely to theory.[55] Figure 21 shows the DC current-voltage characteristics of a high-power (3 Watt CW) 6 GHz GaAs Impatt diode.[34] The device is fabricated using a Pt Schottky barrier and formed in the shape shown in Fig. 20(b). The device operating temperature as a microwave oscillator is 460°K, and the DC measurement at that temperature shows near-ideal current-voltage characteristics, based on the thermionic emmission theory. The breakdown voltage of the same device as a function of heat-sink temperature is shown in Fig. 22 and is also found to be

in good agreement with the theoretical result for one-sided abrupt junctions.[11,56]

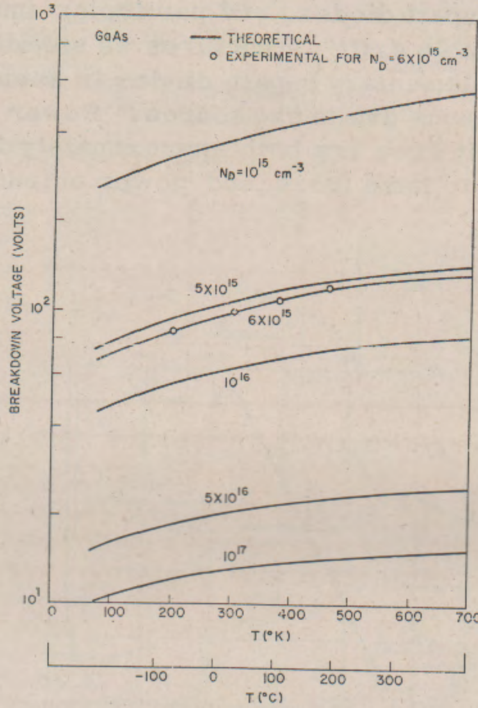

Fig. 22 Breakdown voltage versus temperature follows theory closely. (After Coleman et al., Ref. 55)

2. Frequency Scaling and Microwave Performance

From the small-signal theory we can obtain approximate relations for various device parameters as a function of operating frequency. The conductance expression in Eq. (4) can be rewritten as

$$-G \sim \frac{W^2}{2A\epsilon_s v_s} \left(\frac{1}{\frac{\omega^2}{\omega_r} - 1}\right) \left(\frac{1-\cos\theta}{\theta^2/2}\right) \tag{17}$$

where θ is the transit angle equal to $\omega\tau$ and $\tau \equiv W/v_s$. or -G to be invarient with ω/ω_r, it is required from Eq. (17) that[57]

$$W^2/2A\epsilon_s v_s = \text{constant} \tag{18a}$$

and

$$\omega_r \tau = \text{constant} \tag{18b}$$

ABLE III. APPROXIMATE FREQUENCY SCALING FOR IMPATT DIODES

Parameter	Frequency Dependence
Junction Area, A	f^{-2}
Bias Current Density, J	f
Depletion-Layer Width, W	f^{-1}
Breakdown Voltage, V_B	f^{-1}
Power Output, P_{out}	f^{-1}
Thermal Limitation Electronic Limitation	f^{-2}
Efficiency, η	Constant

Since the depletion width, W, is inversely proportional to the operating frequency (Eq. 6), the device area, which is proportional to W^2, is thus proportional to ω^{-2}. From the avalanche breakdown equation (3a), it can be shown that the ionization rate (α) and its field derivative (α') are inversely proportional to the depletion width. Combination of the relation $\alpha' \sim 1/W$, Eq. (5), and Eq. 18(b), yields the following result for the DC current density

$$J_o \sim \frac{\omega_r^2}{\alpha'} \sim \frac{\omega^2}{1/W} \sim \omega \qquad (19)$$

The above frequency scaling relations are summarized in Table III, and are useful as a guide for extrapolating performance and design to new frequencies.

The power output limitations have been considered in Section IV. The efficiency is expected to be only weakly dependent on frequency at low frequencies. However, at millimeter wave regions the operating current density is high ($\sim f$) and the area is small ($\sim f^{-2}$) so that the device operating temperature will be high. This in turn will cause an increase of the reverse saturation current density and a decrease of the efficiency. In addition, the skin effect, the tunneling effect. and other effects associated with high frequency and high field will also degrade the efficiency performance. Hence, as the frequency increases the efficiency is expected to decrease eventually.

In the low frequency range such as C-band (5-7 GHz) X-band (8-12 GHz) and K-band (18-26 GHz), a useful microwave measurement circuit[58] is shown in Fig. 23. Also shown is a device mounted in a microwave package. For the millimeter wave region both the mounting scheme and

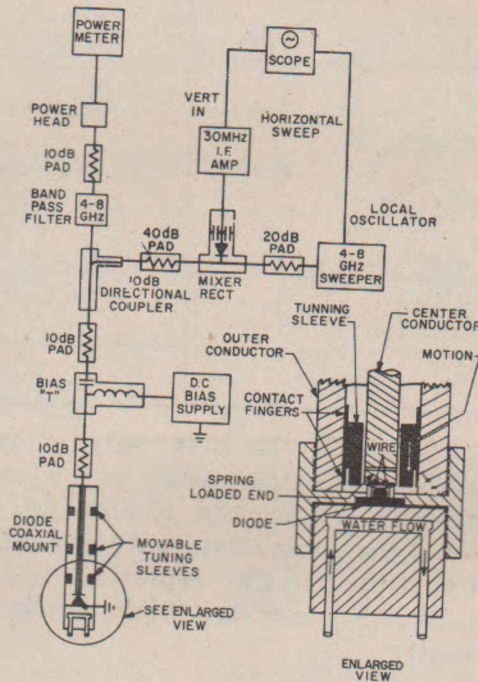

Fig. 23 Drawing of a coaxial oscillation circuit. (After Iglesias, Ref. 58)

microwave circuit should be modified.[59] Typical microwave performances of silicon Impatt diodes are listed in Table IV for three sets of devices.[60] We note that the device parameters follow reasonably close to the frequency scaling listed in Table III. The efficiency in the 100 GHz range is lower presumably due to the aforementioned effects. The relation between the breakdown voltage and frequency is also in good agreement with the computed result shown in Fig. 3.

To demonstrate the importance of the transit-time effect, Fig. 24 shows the breakdown voltage v_B . the optimum frequency at which the efficiency is maximized.[61] The solid lines are calculated from Eq. (6) The agreement is good for all three semiconductors.

Figure 25 compares the performance[59] of double-drift and single-drift diodes at 50 GHz. The double-drift 50 GHz Impatt diode mode by ion implantation shows an output CW power of 1 W with a maximum efficiency of 14%. These results can be compared with a similar single-drift device which delivers about 0.5 W with an efficiency of about 10%.

TABLE IV. DEVICE PARAMETERS AND PERFORMANCE OF EXPERIMENTAL SILICON IMPATT DIODES

Frequency Range	8-10 GHz	50-60 GHz*	100-110GHz
Junction Area (cm^2)	5×10^{-4}	2×10^{-5}	5×10^{-6}
Epitaxial Layer Thickness (μm)	5	2	0.5
Doping Concentration (cm^{-3})	6×10^{15}	6×10^{16}	2×10^{17}
Bias Current Density (A/cm^2)	~1,000	~5,000	~50,000
Depletion-Layer Width (μm)	3.5	0.6	0.25
Breakdown voltage (volts)	85	17	9
Power Output (watts)	3	0.5	0.07
Efficiency	10-12%	10%	3%

*Life test shows that the equivalent life time operated at 200°C is longer than 15,000 hours.

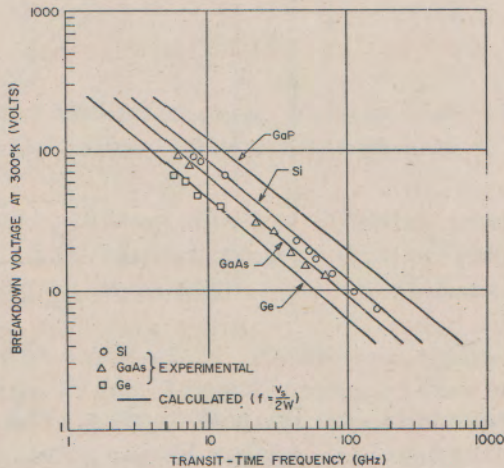

Fig. 24 Calculated breakdown voltage vs frequency for abrupt p-n junction diodes in Ge, Si, GaAs and GaP. Data points are measured results for diodes operated at optimum frequency at which the officiency is maximized. (After Dunn, Ref. 61)

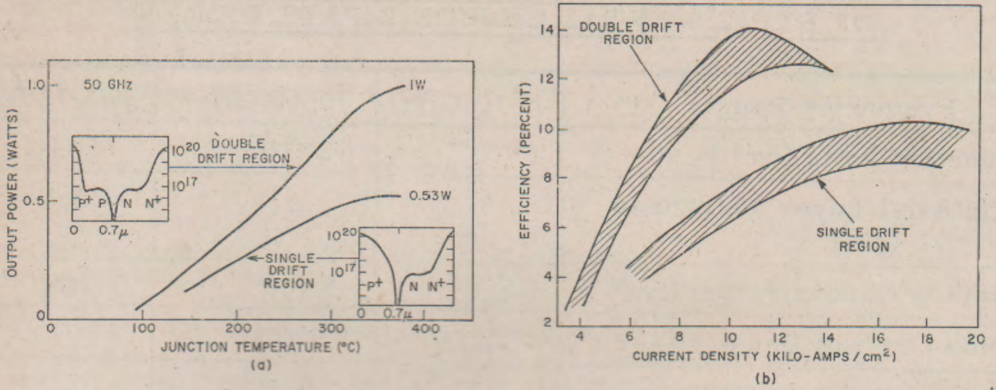

Fig. 25 Power output and efficiency of single-drift versus double-drift Impatt oscillators at 50 GHz. (a) Power output for two individual diodes. (b) Range of efficiency for four diodes of each type. (After Seidel et al., Ref. 59)

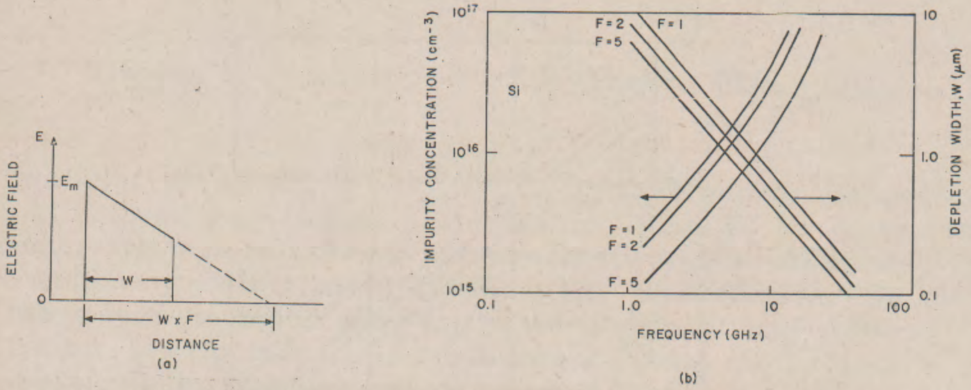

Fig. 26 Design Parameters for Trapatt diodes. The punch-through factor F is defined in (a). (After Evans. Ref. 15 (d))

So far the performance discussion has concerned Impatt diodes. For a Trapatt diode the design and performance are more complicated because of the strong device-circuit interaction which dictates most of the device performance.[15(d)] To reduce the over-voltage, which is the terminal voltage required to initiate the avalanche shock front, a Trapatt diode is

usually designed with a large punch-through factor.[43] The punch-through factor, F, is defined in Fig. 26(a). The larger the factor F, the closer the device resembles a pin diode. The required depletion width and impurity concentration as a function of Trapatt operating frequency is shown in Fig. 26(b) for three punch-through factors.[15(d)]

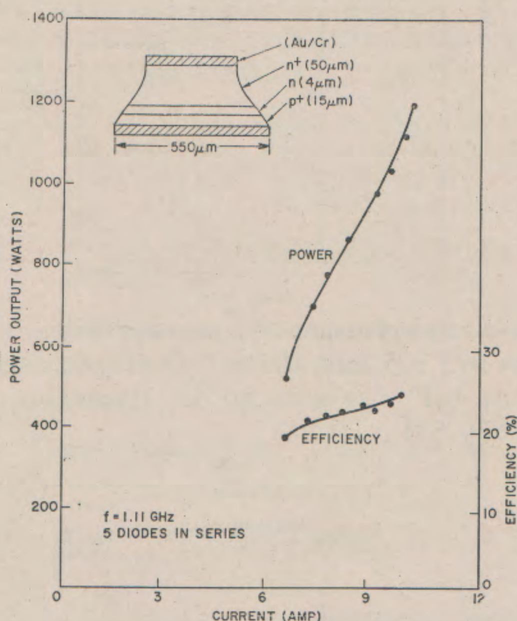

Fig. 27 Power output and efficiency versus current for a stack of 5 diodes at 1.11 GHz. (After Liu and Risko, Ref. 35)

The Trapatt diode state-of-the-art highest power performance is shown[35] in Fig. 27. The output power of a series connection of five diodes under pulse condition reaches 1.2 KW with an efficiency of 25%.

3. State-of-the-Art

A summary of the present state-of-the-art is given in Fig. 28 for Impatt diodes and in Fig. 29 for Trapatt diodes. Also shown in Fig. 28 are the results obtained[19] in 1965. We note there are two to three orders of magnitude in extending the upper frequency limit. The highest Pf^2 CW result was obtained at 50 GHz with a double-drift structure by Seidel, et. al.[59] Most of the data are obtained from silicon avalanche diodes. However, the GaAs 6 GHz Impatt diode, by Irvin, et. al.,[34] exhibits to date the highest CW output power from a single chip. The highest power result under pulse conditions, as mentioned previously, was obtained by Liu, et. al.[35]

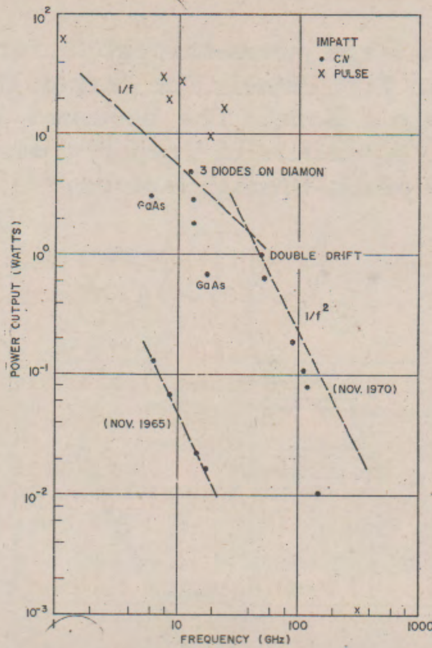

Fig. 28 State-of-the-art performance, power versus frequency, for Impatt diodes in 1965 and 1970. $1/f$ slope is expected for thermal limitation; $1/f^2$ for electronic limitation. (Ref. 19, 34, 48, 53, 60, 62, 63)

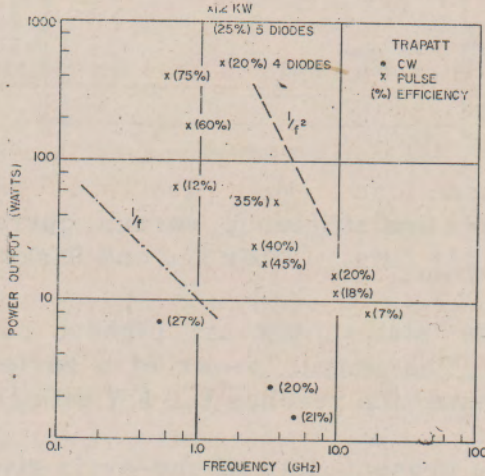

Fig. 29 State-of-the-art, power versus frequency, for Trapatt diodes. (Ref. 35, 40, 66-75)

VIII. ACKNOWLEDGMENTS

We would like to acknowledge the contributions of numerous colleagues at Bell Telephone Laboratories. In particular we wish to thank B. C. DeLoach, Jr., R. Edwards, W. J. Evans, J. C. Irvin, T. Misawa, D. L. Scharfetter, and T. E. Seidel for their published and unpublished work, helpful discussions, and critical reading of the manuscript.

REFERENCES

1. R. L. Johnston, B. C. De Loach, and B. G. Cohen, "A Silicon Diode Microwave Oscillator," Bell Syst. Tech. J., 44, pp. 369-372, February 1965.

2. W. T. Read, "A Proposed High-frequency Negative Resistance Diode," Bell Syst. Tech J., 37, pp. 401-446, March 1958.

3. H. J. Prager, K. K. N. Chang, and S. Weisbrod, "High-Power, High-Efficiency Silicon Avalanche Diodes at Ultra-High Frequencies", Proc. IEEE, 55, pp. 586-587, April 1967.

4. B. C. De Loach, Jr., "Modes of Avalanche Diodes and their Associated Circuits," IEEE, J. Solid State Circuits, SC-4, pp. 101-110, December 1969.

5. S. M. Sze, Physics of Semiconductor Devices, Wiley and Sons, New York, New York, 1969.

6. J. G. Ruch and W. Fawcett, "Temperature Dependence of the Transport Properties of GaAs Determined by the Monte Carlo Method," to be published.

7. V. L. Dalal, "Hole Velocity in p-GaAs," Appl. Phys. Letters, 12, June 15, (1970).

8. E. M. Conwell, High Field Transport in Semiconductors, Academic Press, New York, 1967.

9. C. Y. Duh and J. L. Moll, "Temperature Dependence of Hot Electron Drift Velocity in Silicon at High Electric Fields," Solid State Electrcnics, 11, 917 (1968).

10. G. A. Baraff, "Distribution Functions and Ionization Rates for Hot Electrons in Semiconductors," Phus. Rev., 128, 2507 (1962).

11. C. R. Crowell and S. M. Sze, "Temperature Dependence of Avalanche Multiplication in Semiconductors," Appl. Phys. Letters, 9. 242 (1966).

12. J. L. Moll, Physics of Semiconductors, McGraw Hill Book Co., New York (1964).

13. S. M. Sze and G. Gibbons, "Avalanche Breakdown Voltages of Abrupt and Linearly Graded p-n Junctions on Ge, Si, GaAs and GaP," Appl. Phys. Letters, 8, 111 (1966).

13a. S. M. Sze, M. P. Lepselter, and R. W. MacDonald, "Metal-Semiconductor Impatt Diode," Solid State Electronics 12, 107 (1969).

14. M. Gilden and M. E. Hines, "Electronic Tuning Effects in the Read

Microwave Avalanche Diode," IEEE Trans. on Electron Devices, ED-13, pp. 169-175, January 1966.

14a. H.K. Gummel and D. L. Scharfetter, "Avalanche Region of Impatt Diodes," BSTJ, 45, pp. 1797-1828, December 1966.

15. For a detailed study of the Impatt physics, see, for example, Ref. 5 and the following references:
   (a) J. E. Carroll, Hot Electron Microwave Generators, Edward Arnold (Publishers) Ltd., London, 1970, Ch. 8-10.
   (b) H. A. Watson, Ed., Microwave Semiconductor Devices and their Circuit Applications, McGraw Hill Book Co., 1969, Ch. 15.
   (c) T. Misawa, "Impatt Diodes," a chapter of Semiconductor Applications, which is Vol. 6 in the general series, Semiconductors and Semimetals. Academic Press, New York (1970).
   (d) W. J. Evans, "Avalanche Diode Oscillators," a chapter of Solid State and Quantum Electronics. Edited by W. D. Hershberger, John Wiley and Sons, New York, 1971.

16. T. Misawa, "Negative Resistance in p-n Junctions Under Avalanche Breakdown Conditions," IEEE Trans. on Electron Devices, ED-13 pp. 137-151, January 1966.

17. S. M. Sze and W. Shockley, "Unit Cube Expression for Space-Charge Resistance," Bell Syst. Tech. J. 46, 837 (1967).

18. D. L. Scharfetter and H. K. Gummel, "Large-Signal Analysis of a Silicon Read Diode Oscillator," IEEE Trans. on Electron Devices, Vol. ED-16, pp. 64-77, January 1969.

18a. W. J. Evans and G. I. Haddad, "Large-Signal Analysis of Impatt Diodes," IEEE Trans. on Electron Devices, ED-15, pp. 708-717, October 1968.

18b. J. L. Blue, "Approximate Large-Signal Analysis of Impatt Oscillators," BSTJ, 48, pp. 383-396, February 1969.

19. B. C. De. Loach, Jr., "Recent Advances in Solid-State Microwave Generators," Advances in Microwaves, Vol. II, Academic Press, Inc., New York, 1967.

20. C. B. Swan, T. Misawa, and L. P. Marinaccio, "Composite Avalanche Diode Structures for Increased Power Capability," IEEE Trans. on Electron Devices, ED-14, pp. 584-589, September 1967.

21. G. Gibbon and T. Misawa, "Temperature and Current Distribution in an Avalanching p-n Junction," Solid State Electronics, 11. 1007 (1968).

22. R. H. Haitz, H. L. Stover, and N. J. Tolar, " A Method for Heat Flow Resistance Measurements in Avalanche Diodes," IEEE Trans. on Electron Devices, Vol. ED-16, pp. 438-444, May 1969.

23. D. L. Scharfetter, "Power-Impedance-Frequency Limitations of Impatt Oscillators Calculated from a Scaling Approximation," Proc. IEEE, this issue.

24. T. Misawa, "Saturation Current and Large Singnal Operation of a Read Diode," Solid State Electronics 13, 1363 (1970).

25. D. R. Decker, C. N. Dunn, and H. B. Frost, "The Effect of Injecting Contacts on Avalanche Diode Performance," to be published.

26. S. R. Kovel and G. Gibbons, "The Effect of Unswept Epitaxial Material on the Microwave Efficiency of Impatt Diodes," Proc. IEEE, 55, pp. 2066-2067, November 1967.

27. B. C. De Loach, Jr., "Thin Skin Impatts," IEEE G-MTT, MTT-18, pp. 72-74, January 1970.

28. C.Y.Chang and S. M. Sze, "Carrier Transport Across Metal-Semiconductor Barriers." Solid State Electronics 13, 727 (1970).

29. T. Misawa, private communication.

30. M. E. Hines, "Noise Theory for the Read Type Avalanche Diode," IEEE Trans. on Electron Devices, ED-13, p. 158. January 1966.

31. H. K. Gummel and J. L. Blue, "A Small-Signal Theory of Avalanche Noise in Impatt Diodes," IEEE Trans. on Electron Devices, ED-14, pp. 569-580, September 1967.

32. J. L. Blue, "Preliminary Theoretical Results on Low Noise GaAs Impatt Diodes," IEEE Device Research Conference, Seattle, June (1970).

32a. P. A. Levine, "Ultralow Noise in Pulsed GaAs Avalanche Diode Oscillators," Proc. IEEE, 58, 495 (1970).

33. J. G. Josemhans, private communications.

34. J. C. Irvin, D. J. Coleman, W. A. Johnson, I. Tatsuguchi, D. R. Decker, and C. N. Dunn, "Fabrication and Noise Performance of High-Power GaAs Impatts," IEEE International Electron Device Metting, Washington, D.C., October 28, 1970. (paper 8.8).

35. S. G. Liu and J. J. Risko, "Fabrication and Performance of Kilowatt L-band Avalanche Diodes," RCA Review, Vol. 31, 3, (March 1970).

36. D. F. Kostichack, "UHF Avalanche Diode Oscillator Providing 400 Watts Peak Power and 75 Percent Efficiency," Proc. IEEE, 58, pp. 1282-1283, August 1970.

37. D. L. Scharfetter, D. J. Bartelink, H. K. Gummel and R. L. Johnston, "Computer Simulation of Low Frequency High Efficiency Oscillation in Germanium," IEEE Solid State Device Research Conference, June 17-19, 1968. Also IEEE Trans. Electron Devices, ED-15, p. 691, September 1968.

38. R. L. Johnston, D. L. Scharfetter, and D. J. Bartelink, " High-Efficiency Oscillations in Germanium Avalanche Diodes Below the Transit-Time Frequency, Proc. IEEE, 56, pp. 1611-1613, September 1968.

39. D. J. Bartelink and D. L. Scharfetter, "Avalanche Shock Fronts in p-n Junctions," Appl. Phys. Lett., May 15, 1969.

40 A. S. Clorfeine, R. J. Ikola, and L. S. Napoli, "A Theory for the High-Efficiency Mode of Oscillation in Avalanche Diodes," RCA Review, pp. 397-421, September 1969.

41. B. C. De Loach, Jr., and D. L. Scharfetter, "Device Physics of Trapatt Oscillators," IEEE Trans. on Electron Devices, ED-17, January 1970, pp. 9-21.

42. W. J. Evans, "Circuits for High Efficiency Avalanche Diode Oscillators," IEEE Trans. Microwave Theory and Techniques, MTT-17, pp. 1060-1067, December 1969.

43. D. L. Scharfetter, "Power-Frequency Characteristics of the Trapatt Diode Mode of High Efficiency Power Generation in Germanium and Silicon Avalanche Diodes," Bell Syst. Tech. J., 49, 799 (1970).

44. B. C. De Loach and R. L. Johnston, "Avalanche Transit-Time Microwave Oscillators and Amplifiers," IEEE Trans. on Electron Devices, Vol. ED-13, pp. 181-186, January 1966.

45. B. Hoefflinger, C. P. Snapp, and L. A. Stark, High-Efficiency Avalanche Resonance Pumped Amplification," IEEE J. Solid State Circuits, SC-4, pp. 391-395, December 1969.

46. D. L. Scharfetter, D. J. Bartelink and B. C. De Loach, "Comments on Static Negative Resistance in Avalanche Silicon p -i-n Junctions," IEEE Trans. Electron Devices, ED-16, pp. 920-972, November 1969.

47. T. Misawa, "Microwave Si Avalanche Diode with Nearly-Abrupt-Type Junction," IEEE Trans. on Electron Devices, Vol. ED-14, pp. 580-584, September 1967.

47a. T. Misawa, "CW Millimeter-Wave Impatt Diodes with Nearly Abrupt Junctions," Proc. IEEE, Vol. 56, pp. 234-235, February 1968.

47b. R. A. Zettler and A. M. Cowley, "Batch Fabrication of Integrated-Heat-Sink Impatt Diodes," Electronic Letters, 5, No. 27, December 1969.

48. R. Edwards, D. F. Ciccolella, T. Misawa, D. E. Iglesias and V. Decker, "Millimeter-Wave Silicon Impatt Diodes," International Electron Devices Meeting, October 29-31, 1969.

49. D. DeNoble and H. G. Kock, "A Silicon Schottky Barrier Avalanche Transit Time Diode." Proc. IEEE 57, pp. 2088-2089, November 1969.

50. C. K. Kim and L. D. Armstrong, "GaAs Schottky-Barrier Avalanche Transit Time Diode." Solid State Electronics, 13, 53-56, January 1970.

50a. Y. S. Lee and C. K. Kim, "Two-Watt CW GaAs Schottky-Barrier Impatt Diodes," Proc. IEEE 58, pp. 1113-1154, July 1970.

51. T. Misawa, "Theoretical Study of Microwave Oscillation Efficiency in Improved Read Diodes," to be published.

52. T. Misawa, "Minority Carrier Storage and Oscillation Efficiency in Read Diodes," Solid State Electron, 13, 1369 (1970).

53. D. L. Scharfetter, W.J. Evans, and R. L. Johnston, "Double-Drift -Region (p pnn) Avalanche Diode Oscillators," Proc. IEEE 58, 1131 (1970).

54. T. Seidel and P. L. Scharfetter, "High-Power Millimeter Wave Impatt Oscillators with Bosh Hole and Electron Drift Space made by Ion Implantation," Proc. IEEE 58, 1135 (1970).

55. D. J. Coleman, J. C. Irvin, and S. M. Sze, "GaAs Schottky Diodes with Near Ideal Characteristics," to be published.

56. Y. Y. Chang and S. M. Sze, "Temperature Dependence of Ionization Rates in GaAs," J. Appl. Phys. 40, 5392, (1969).

57. F. A. Blum and N. B. Kramer, "Frequency Scaling of Impatt Diodes," IEEE Trans. on Electron Devices, Ed-17, pp. 983-986, November 1970.

58. D. E. Iglesias, "Circuit for Testing High-Efficiency Impatt Diodes," Proc. IEEE, Vol. 55, pp. 2065-2066. November 1967.

59. T. E. Seidel, R. E. Davis and D. E. Iglesias, "Double-Drift-Region Ion-Implanted Millimeter-Wave Impatt Diodes, " Proc. IEEE, this issue.

60. T. Misawa and L. P. Marinaccio, "100 GHz Si Impatt Diodes for CW Operation," to be published.

61. C. N. Dunn, "Empirical Transit-Time-Frequency-Breakdown Voltage Curves for Impatt Diodes," to be published.

62. S. G. Liu, J. J. Risko, and K. K. N. Chang, "High-Power K-Band Silicon Avalanche Diode Oscillators," Proc. IEEE, Vol. 58, pp.

919-920, June 1970.

63. C. B. Swan, "Improved Performance of Silicon Avalanche Oscillator Mounted on Diamond Heat Sinks,"IEEE Proc. (Letters), Vol. 55, pp. 1617-1618. September 1967.

64. C. B. Swan, T. Misawa, and C. H. Bricker, " Continuous Oscillations at Millimeter Wavelengths with Silicon Avalanche Diodes," Proc. IEEE, Vol. 55, pp. 1747-1749, October 1967.

65. L. S. Bowman and C. A. Burrus, "Pulse-Driven Silicon p-n Junction Avalanche Oscillators for the 0.9 to 20 mm Band," IEEE Trans. on Electron Devices, Ed-14, August 1967, pp. 411-418.

66. G. Gibbons and M. I. Grace, "High-Efficiency Avalanche-Diode Oscillators and Amplifiers in X-Band," Proc. IEEE (Letters), Vol. 58, pp. 512-513, March 1970.

67. R. S. Ying, R. G. Mankariour, and D. L. English, " High-Efficiency Anomalous Mode Oscillation from Silicon Impatt Diodes at 6 GHz," 1969 ISSCC Digest, pp. 86-87.

68. W. J. Evens and D. E. Iglesias, "CW Silicon Trapatt Operation," Proc. IEEE, Vol. 58, pp. 285-286, Frbruary 1970.

69. D. E. Iglesias and W. J. Evans, " High Efficiency CW Impatt Operation," Proc. IEEE (Letters), Vol. 56, p. 1610, September 1968.

70. W. J. Evans and R. L. Johnston, "Improved Performance of CW Silicon Trapatt Oscillators," Proc. IEEE (Letters), Vol. 58, pp. 846-846, May 1970.

71. W. J. Evans, T. E. Seidel, and D. L. Scharfetter, "A Novel Trapatt Oscillator Design," Proc. IEEE 58, pp. 1294-1295, August 1970.

72. R. S. Ying and N. B. Kramer, "X-Band Silicon Trapatt Diodes," Proc. IEEE 58, pp. 1285-1286, August 1970.

73. R. J. Chaffin and G. P. EerNisse, " A Poor Man's Trapatt Oscillator," Proc. IEEE 58, 173, January 1970.

74 M. Yeon Ta, "High-Power Subharmonic Oscillation in Silicon Avalanche Diodes at Ku Band," Proc. IEEE 57, 2054 (1969).

75. S. G. Liu, "Stacked High Power Avalanche - Diode Oscillators," Proc. IEEE, 57, 707 (1969).